Available online at www.sciencedirect.com
SCIENCE DIRECT®
Journal of Power Sources 119–121 (2003) 266–272
JOURNAL OF POWER SOURCES
www.elsevier.com/locate/jpowsour

Performance characteristics of lithium vanadium phosphate as a cathode material for lithium-ion batteries

M.Y. Saïdi[*,1], J. Barker[1], H. Huang, J.L. Swoyer[1], G. Adamson

Valence Technology Inc., 301 Conestoga Way, Henderson, NV 89015, USA

Abstract

The properties of the monoclinic lithium vanadium phosphate, $Li_3V_2(PO_4)_3$ (LVP), are investigated using X-ray diffraction (XRD) and electrochemical methods. Electrochemical measurements conducted in half cells with $Li_3V_2(PO_4)_3$ as the cathode material and lithium metal as the anode have shown that this material exhibits an excellent reversibility when the charge extracted is confined to that equivalent to two lithiums per formula unit. The extraction of the last lithium is observed at a potential >4.6 V versus Li/Li^+ and involves a significant overvoltage. Upon discharge, a solid solution behavior is observed after which the two-phase regime for the last lithium insertion reappears. Furthermore, XRD has shown that the original structure is recovered. Cycling performance as well as rate capability are also presented for rocking-chair batteries based on LVP and graphite.

Keywords: Lithium vanadium phosphates; Lithium batteries; Intercalation; Structure

1. Introduction

Transition metal oxides and chalcogenides with layered and three-dimensional (3D) frameworks have been the focus of a wide development effort as cathodes materials for lithium rechargeable batteries [1–3]. Considerable study has also been given to lithium conducting phosphates, $Li_3M_2(PO_4)_3$, and materials based on these compounds [4,5]. Their structural type allows various isomorphous replacements, which are of importance in increasing the concentration of lithium or selecting the optimal dimensions of the conductivity channels for example. Recently, we have undertaken a general study of phosphates and vanadates with the general formula $Li_3M_2(PO_4)_3$. Such framework structures containing an interconnected interstitial space are potentially fast ionic conductors, especially if the energetically equivalent sites are connected. The substitution of the larger poly-anion, instead of the smaller O^{2-} ions, in an open 3D framework helps to stabilize the structure and allows a faster ion migration. Furthermore, anion substitution can alter the voltage through two effects; the first is an inductive one due to changes in the metal ion energy levels because of the changed anion group. The second effect is possibly achieved by providing fewer or more electrons, thereby shifting the lithium concentration at which a given redox reaction takes place. For example, in $Li_xV_2(XO_4)_3$, the $V^{3+/4+}$ redox couple takes place for $x = 1$–3 (X = P) or $x = 4$–6 (X = Si) depending on the poly-anion unit chosen. A number of these phosphates such as $M_2(XO_4)_3$ have been reported to be stable in total absence of alkali cations such as molybdates and tungstates of M = Sc^{3+}, Cr^{3+}, Fe^{3+}, etc. These crystallize in an orthorhombic symmetry [6–8]. The vanadium phosphate in particular, $V_2(XO_4)_3$ preparation has been reported via a chemical route [9] by removal of all the sodium from the $Na_3V_2(PO_4)_3$ nasicon phase. The $V_2(PO_4)_3$, thus obtained possesses the same hexagonal structure as the parent compound $Na_3V_2(PO_4)_3$ with minor changes in the lattice parameters. However, Goodenough and co-workers [10] found that they could only remove two sodiums chemically.

We have previously investigated the vanadium nasicon related $Li_xV_2(XO_4)_3$ compound and found that two lithiums could reversibly be cycled over the range of 3–4.3 V [11]. Since the $V^{3+/4+}$ redox couple takes place at 3.5 and 4 V, it suggests that the $V^{4+/5+}$ is quite high. We have in this work attempted to extract the remaining lithium electrochemically.

2. Experimental

The lithium vanadium phosphate was prepared by mixing stoichiometric amounts of $NH_4H_2PO_4$, V_2O_5, and Li_2CO_3.

* Corresponding author.
E-mail address: yazid.saidi@valence.com (M.Y. Saïdi).
[1] Electrochemical Society active member.

0378-7753/03/$ – see front matter © 2003 Published by Elsevier Science B.V.
doi:10.1016/S0378-7753(03)00245-3

The mixture was initially heated to 300 °C in air for 4 h to allow H_2O and NH_3 to evolve. The resulting product was then ground, pelletized, and heated to 850 °C under a stream of pure hydrogen for 8 h. Once the furnace had cooled down, the latter process was repeated for a further 16 h to ensure completion of the reaction. Materials used to collect data for this work were synthesized following this route. An alternative preparation method involved carbo-thermal reduction (CTR) using carbon as the reducing agent. A previous paper by this group [18] detailed the use of a carbo-thermal reduction (CTR) method to synthesize a range of lithiated transition metal compounds, including poly-anion and oxide based materials.

The $Li_3V_2(PO_4)_3$ electrodes were prepared by mixing with Super P and PVDF copolymer (polyvinylidene fluoride) in acetone to ensure homogeneity. The resulting slurry was coated on aluminum foil placed on a glass plate using a doctor blade. After the acetone had evaporated, the resulting electrode composition was 80:10:10 of active material, Super P (Erachem, Belgium) and PVDF–HFP, Kynar 2801 copolymer (Atofina), respectively. A glass fiber separator was placed between the $Li_3V_2(PO_4)_3$ electrode and lithium metal was used as the anode. The electrolyte used consisted of a 1 M solution of $LiPF_6$ in a mixture of 2:1 by weight of ethylene carbonate (EC) and dimethyl carbonate (DMC) and 1:1 for the rate capability measurements. Cycling tests were carried out at a current of 0.2 mA/cm^2 for charge and discharge, respectively, between 3.0 and 4.2, or 5.0 V depending on the charge regime. To monitor changes in the $Li_3V_2(PO_4)_3$ structure during cycling, X-ray diffraction (XRD) was performed at two different states of charge: fully charged to 5.0 V (versus Li/Li$^+$) and fully discharged to 3.0 V (versus Li/Li$^+$). Fully charged or discharged cells were allowed to equilibrate before they were moved to an argon filled glove box where the electrode was removed from the cell pouch and rinsed with DMC solvent in order to remove any residual salt. The electrode was then covered with X-ray amorphous tape to prevent any moisture intrusion and later transferred to a Siemens D5000 X-ray diffractometer.

Electrochemical properties of the test materials were initially evaluated using a commercial battery cycler in lithium metal and rocking-chair configuration. The positive electrodes comprised 84-wt.% active materials, 5-wt.% Super P (conductive carbon) and 11-wt.% PVdF–HFP co-polymer (SOLEF, Solvay Chemical) binder. Life cycling experiments were performed in conventional small prismatic cells using the same positive electrode stock. Advanced performance characteristics of the active materials were determined in a lithium-ion configuration, using a capacity-balanced microbead type graphite (MCMB2528 from Osaka Gas, Japan) as the negative active material. A typical cell comprised 30 mg of active LVP and 22.2 mg of active graphite for a final balance of 1.8:1. The negative electrodes comprised 84-wt.% active materials, 5-wt.% Super P and 11-wt.% of the PVdF–HFP co-polymer binder. The lithium half-cells were tested at a typical current density of 0.2 mA/cm^2 ($\approx C/8$), whereas the rocking-chair type cells were tested at $C/5$ rate.

3. Results and discussion

The initial characterization of the material was carried out using powder X-ray diffraction (XRD). The pattern shown in Fig. 1(a) is consistent with that previously published [10]. A least square refinement of the XRD pattern using the *hkl* indices for space group #14 ($P2_1/n$) gave the following unit-cell parameters, with the estimated standard deviations shown in parenthesis, Table 1. Fig. 1(b) is the simulated XRD pattern using the above structural parameters and the associated atoms positions [16]. The structure consists of a 3D framework of metal octahedra and phosphate tetrahedra sharing oxygen vertices. Each metal M-octahedron is surrounded by six P-tetrahedra, whereas each tetrahedron is surrounded with four M-octahedra. This configuration forms a 3D network of M_2T_3 units. The Li-atoms, are located in the cavities within the framework. Three four-fold crystallographic positions exist for the lithium atoms leading to 12 lithium positions within the unit-cell. The lantern unit representation of the monoclinic structure of $Li_3V_2(PO_4)_3$ is shown in Fig. 2 with the general Li positions also highlighted.

The electrochemical data was collected with lithium based cells. Electrochemical voltage spectroscopy, EVS [12,13] was used in obtaining the voltage profiles, which at the rates used ($\approx C/20$) provides a high approximation to

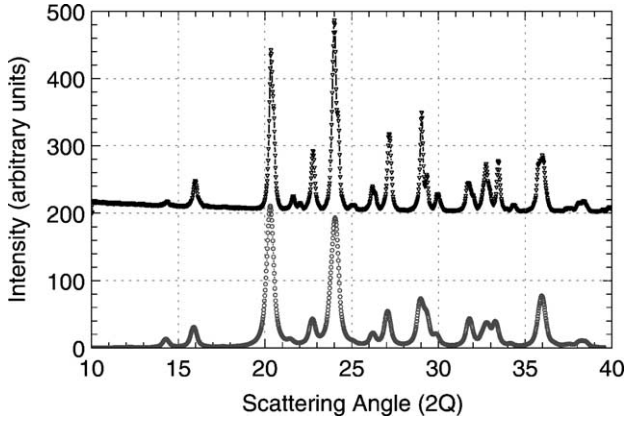

Fig. 1. (a) (△) Experimental XRD pattern of $Li_3V_2(PO_4)_3$; (b) (○) simulated XRD pattern.

Table 1
Unit-cell parameters for $Li_3V_2(PO_4)_3$

a (Å)	b (Å)	c (Å)	β (°)	V/FU (Å^3)	Z	ρ (g/cm^3)
8.662 (2)	8.624 (2)	23.104 (1)	90.452 (2)	226.04	4	3.0

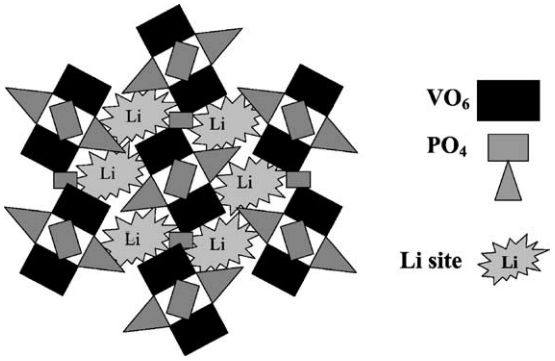

Fig. 2. View of the lantern unit configuration (*a*-axis projection) in $Li_3V_2(PO_4)_3$.

the open circuit voltage. The resulting differential capacity has been shown to allow effective characterization of order–disorder and structural ordering phenomenon in intercalation systems [14,15]. Both voltage profile and differential capacity are shown in Figs. 3 and 4.

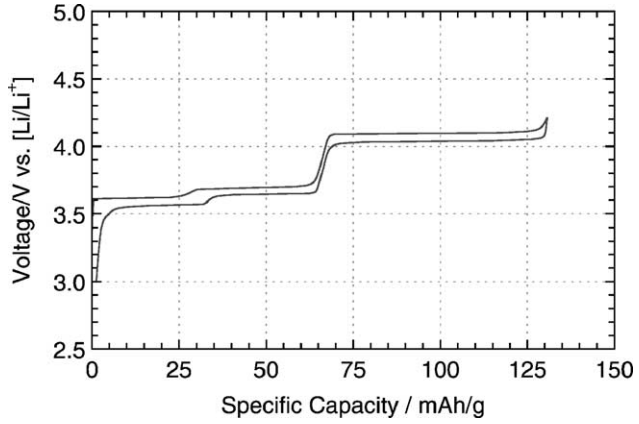

Fig. 3. EVS voltage profile of $Li_3V_2(PO_4)_3$ between 3 and 4.3 V vs. Li/Li^+.

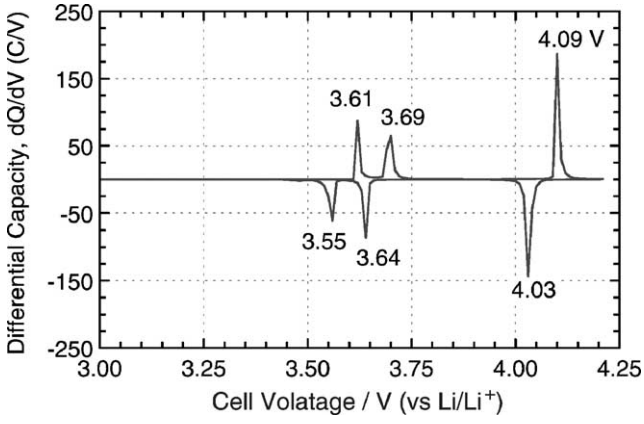

Fig. 4. Differential capacity plot of a $Li/Li_3V_2(PO_4)_3$ cell (derived from data in Fig. 3).

In order to guide us in our investigation, the experimental titration curve for $Li_3V_2(PO_4)_3$ is broken into three regions. These regions span the following composition ranges; $x = 0$–0.5, 0.5–1 and 1–2 in $Li_{(3-x)}V_2(PO_4)_3$, respectively. In each region, plateaus are observed, substantiating the two phase character of the electrochemical reaction in this range, with little or no lithium solubility in each phase. Under the current regime used, the first two lithiums are extracted at an average voltage of 3.64 and 4.08 V versus Li/Li^+, respectively. In turn, the first lithium is removed in two steps, i.e. 3.60 and 3.68 V versus Li/Li^+. This is because of the presence of an ordered Li phase at $x = 2.5$ in $Li_xV_2(PO_4)_3$. The second lithium, however, is extracted over one single step, 4.08 V versus Li/Li^+. The discharge following removal of the first two lithiums, shows a small hysterisis underlying the high reversibility of the system as an active material for lithium-ion batteries. Almost all of the lithium equivalents to 2 mol/FU has been extracted (130 mAh/g) for a theoretical capacity of 133 mAh/g followed by a discharge capacity of 128 mAh/g. Both plateaus correspond to lithium extraction associated with the V^{3+}/V^{4+} redox couple. Since the removal of the second lithium, observed at the higher voltage of 4.1 V (versus Li/Li^+), is associated with the V^{3+}/V^{4+} couple, the corresponding sites associated with the removal of the second lithium are more stable (lower energy) than those coupled with the first lithium. The details of the structural analysis of this system will be made available in an extended publication [16].

Extraction of all the lithium from the lithium vanadium phosphate has been carried out electrochemically up to 5 V versus Li/Li^+. The associated voltage profile is shown in Fig. 5. As mentioned earlier, the first two lithiums are extracted below 4.3 V as shown in Fig. 4, together with the associated capacity with each step up to 5 V. The extraction of the third lithium, associated with the V^{4+}/V^{5+} redox couple, occurs at 4.55 (versus Li/Li^+) and, as seen, is coupled with a significant overvoltage, suggesting the higher energetics involved in removing the last lithium

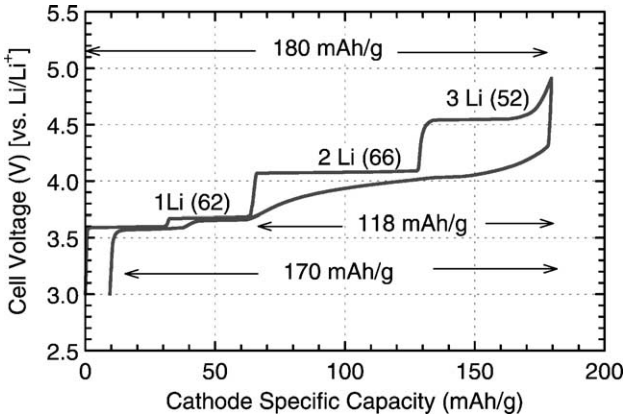

Fig. 5. EVS voltage profile of $Li_3V_2(PO_4)_3$ between 3 and 5.0 V vs. Li/Li^+.

from its site. From the longer equilibration times observed during the EVS experiments, it is suggested that the lithium-ion diffusion rate is initially fast and decreases only when $x > 2$ in $Li_{3-x}V_2(PO_4)_3$. The longer equilibration time in this region indicates that there are regions within the electrode where the mobility of the two-phase interface is slow. Furthermore, the nucleation of the second phase and the slower kinetics support the suggestion of a smaller interface area and a diminishing fraction of the more mobile interfaces. The discharge step, on the other hand, exhibits an almost 0.5 V drop. We believe that during discharge from $x = 0$, there is initially a structural change that creates significantly different Li environments than those seen upon charging [16]. This drop is followed by a single phase region. This region spans the insertion of the equivalent of two lithiums approximately (total of 118 mAh/g). When compared to the capacity extracted upon charge, the extraction of the last two lithiums is fully reversible ($66 + 52$ versus 118 mAh/g). The last step, consisting of the re-insertion of the last lithium, $Li_2V_2(PO_4)_3 \rightarrow Li_3V_2(PO_4)_3$, shows a partial loss and exhibits its characteristic two-phase behavior. Its associated plateau is centered on the lower voltage of 3.61 V instead of 3.64 V versus Li/Li^+ with a small reduction in the reversible charge return. Still, the equivalent capacity on discharge shows that extraction of the third lithium, i.e. $Li_1V_2(PO_4)_3 \rightarrow V_2(PO_4)_3$ is reversible and under the test conditions used an equivalent of 170 mAh/g was re-inserted back into the LVP structure. The features in the voltage profile are better depicted in the differential capacity plot. The single phase portion from the voltage profile, $Li_3V_2(PO_4)_3 \rightarrow Li_1V_2(PO_4)_3$ is shown as a featureless portion in the differential capacity plot, Fig. 6.

The XRD diagram at the end of charge, and discharge following extraction of three lithiums per formula unit, is presented in Fig. 7. The amorphous edge present at the start of the scan is due to the tape used to prevent moisture intrusion during data collection. The observed broadening

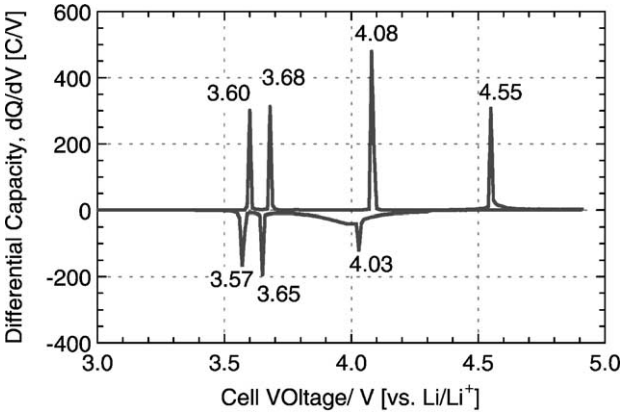

Fig. 6. Differential capacity plot of a $Li/Li_3V_2(PO_4)_3$ cell (derived from data in Fig. 5).

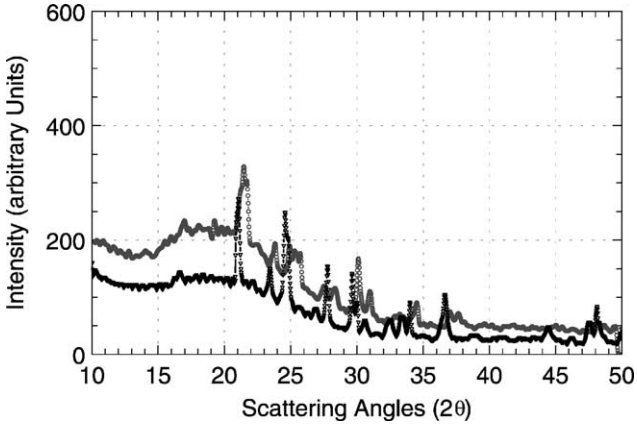

Fig. 7. (○) XRD pattern of charged LVP cathode to 5 V (vs. Li/Li^+); (△) subsequent discharge to 3 V vs. Li/Li^+.

of the peaks might be associated with a partial material decomposition. The de-lithiated LVP phase, $V_2(PO_4)_3$ phase, shows a similar pattern to that of the original monoclinic phase. The adoption of this monoclinic structure has also been observed in the case of the nasicon related iron sulfates; $Fe_2(SO_4)_3$ and $FeTi(SO_4)_3$, [17]. Upon discharge, the original monoclinic structure of the lithium vanadium phosphate, $Li_3V_2(PO_4)_3$, is recovered.

Initial cycling experiments, conducted at *C*/5 charge and discharge, were performed using lithium metal as the negative electrode. These experiments were intended to depict the numerous features in the voltage profile during the electrochemical titration step. This involved extraction of 2, 2.5, and 3 lithiums (or equivalent). Fig. 8a-c illustrate the steps involved in the extraction and insertion reactions. Both the 2 and 2.5 lithium profiles show similar steps and the two-phase behavior observed in the case of $Li_3V_2(PO_4)_3 \rightarrow Li_1V_2(PO_4)_3$ is preserved. We have confirmed that the unique voltage profile features observed in the subsequent discharge (see Fig. 5) when the equivalent of 3 lithiums are extracted occurs when $x > 2.5$ Li in $Li_{3-x}V_2(PO_4)_3$. This transition coincides with a shift from a two-phase to a single-phase behavior, as observed at the end of charge, Fig. 5. The same voltage profile features are also depicted in a rocking-chair configuration, where the LVP material was coupled with a capacity matched graphite, MCMB 25–28 (Osaka Gas). The cell was charged under constant current conditions at a *C*/5 rate charge and discharge. The first charge inefficiency amounts to around 14%, a figure somewhat higher than what is reported in commercial lithium-ion cells. However, this figures includes the loss associated with the cathode itself, as observed during the EVS electrochemical testing results, as well as that associated with the anode. As expected, the step behavior in the voltage profile of the LVP based electrode is maintained, however, it is now less structured due to the graphite contribution, Fig. 9. The charge and discharge capacities amounted to 175 and 151 mAh/g, respectively, under the prevailing test conditions (*C*/5).

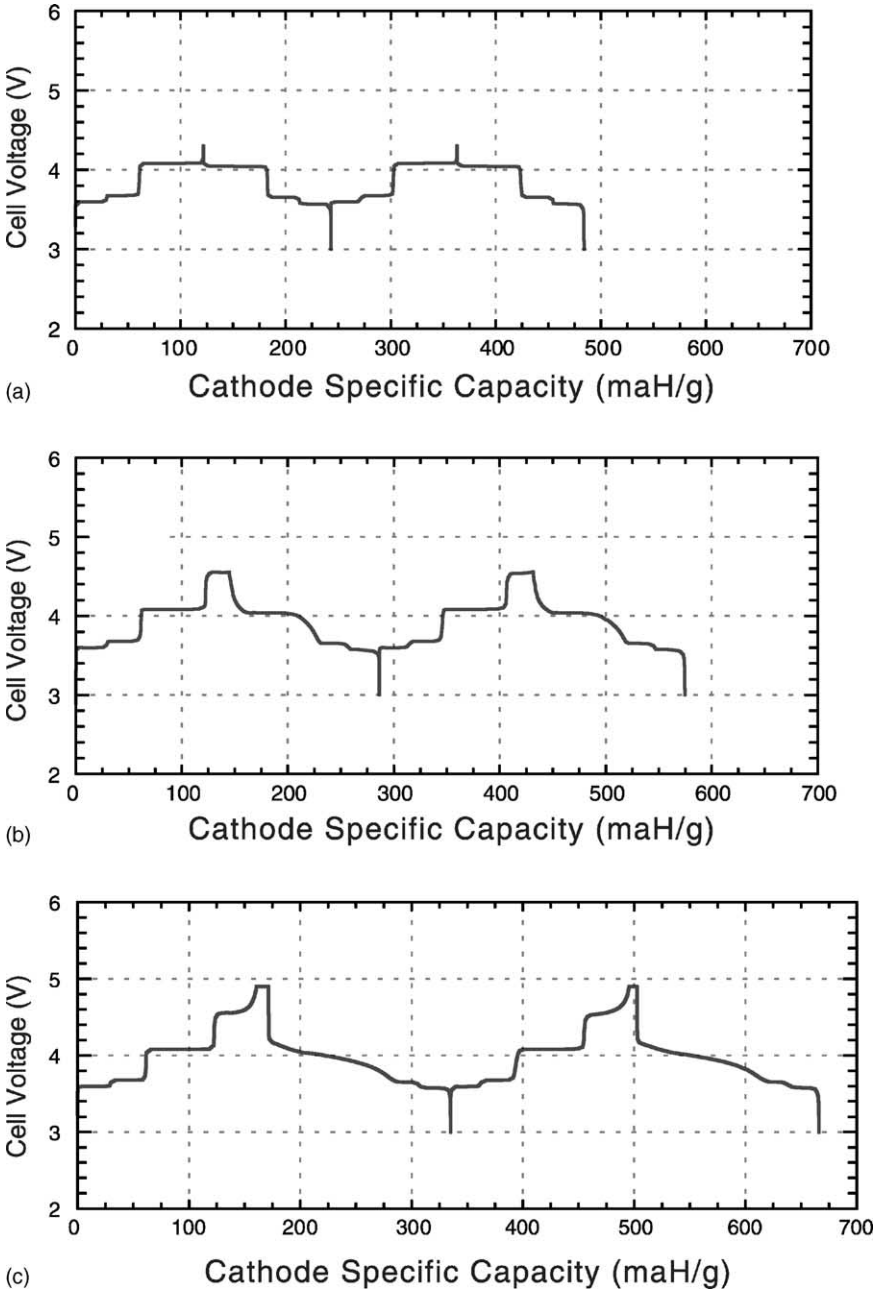

Fig. 8. LVP||Li half cells voltage profiles: (a) 30–4.3, (b) 3.0–4.5 and (c) 3.0–4.8 V.

The rate capability is understood to be very important if commercially viable systems are to be developed. In this context, rate capability refers to the ability of an electrode material to retain its capacity when discharged under different rates, sometimes specified at a given temperature. The rocking-chair cell configuration was chosen for this test and equivalent cells based on $LiCoO_2$ (LCO) were also used for a comparative analysis. All cells were initially cycled three times before the test was performed. Two rates were used, *C*/5 and *C*/2 at 23 °C. Furthermore, adequate low temperature performance is a key requirement for energy storage devices. The electrolyte composition usually plays an important role in determining the limiting step both from an ionic conductivity as well as its ability to form an effective SEI layer on carbon–graphite anode and to some extent on the surface of the cathode electrode. The rocking-chair configuration test was conducted at −10 °C (*C*/2) and used 1 m $LiPF_6$ in 1:1 EC:DMC electrolyte. The discharge characteristics of the cells are illustrated in Figs. 10 and 11. The gravimetric energy density for the lithium vanadium phosphate is approximately 10% higher than that of LCO at 23 °C. The theoretical volumetric energy density for LVP

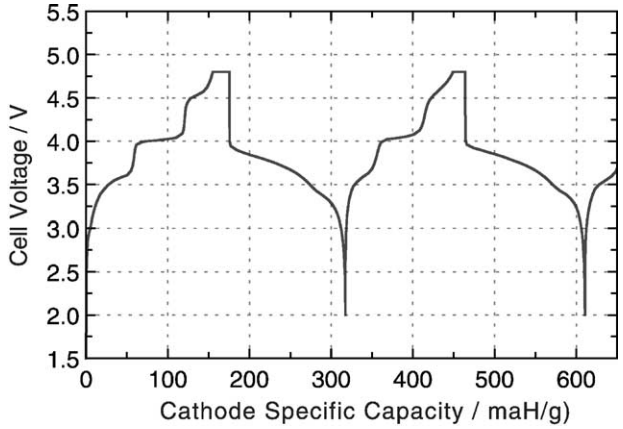

Fig. 9. Voltage curve for LVP||graphite cell at *C*/5 rate between 3.0–4.8 V.

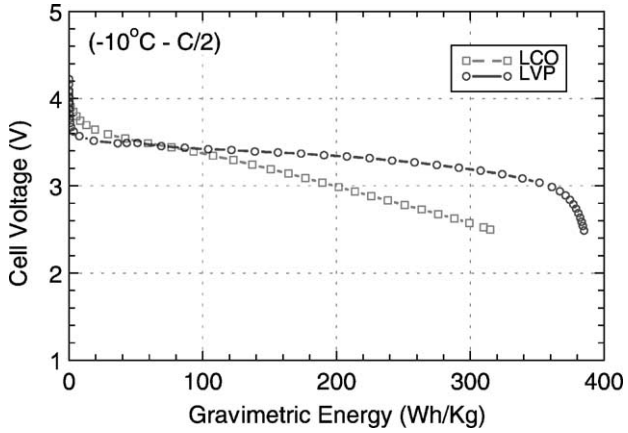

Fig. 11. Discharge curves for LVP||graphite and LCO||graphite cells at *C*/2 (−10 °C).

would be lower than that of say LCO, by virtue of the lower true density. However, cell design and electrode engineering have a greater influence on the final volumetric energy density (Wh/l) figures. The difference in performance at −10 °C is even greater (≈20%) and amounts to 393 versus 315 Wh/kg for $Li_3V_2(PO_4)_3$ and $LiCoO_2$, respectively, underlying the greater ability of LVP to store and release energy at low temperatures. Moreover, the less sloping voltage under the higher current drain allows for maximum energy and efficiency, Fig. 11.

The charge–discharge profiles of rocking-chair LVP, coupled with graphite, cells cycled at room temperature is shown in Fig. 12. As mentioned earlier the voltage cut-offs were chosen so as to remove the equivalent of 2, 2.5 and 3 lithiums equivalents. At the end of the charge process, the voltage was held until the current decreased to 10% of its original value before the discharge proceeded. The discharge capacities obtained for each case include losses associated with each step as well as the loss due to the formation of the SEI layer on the carbon anode. A more sustained cycling behavior is observed for the 4.3 and 4.5 V voltage cut-offs with good specific capacities of 110 and 135 mAh/g, respectively, in a lithium-ion cell.

Safety combined with thermal stability in the charged state are two important factors when developing cathode materials with high energy density. Differential scanning calorimetry (DSC) offers a convenient means of studying the stability of charged cathodes under controlled conditions and reflects the reactivity of the material towards its environment (electrolyte). Heat flow was detected over the temperature range of 220–250 °C as two separate events. The combined exotherm amounted to 239 J/g, Fig. 13. When compared to other charged $Li_{0.5}NiO_2$ and $Li_{0.5}CoO_2$, and λ-MnO_2 cathodes with respective heat flows of 890, 570 and 340 J/g, the lithium vanadium phosphate offers excellent thermal stability.

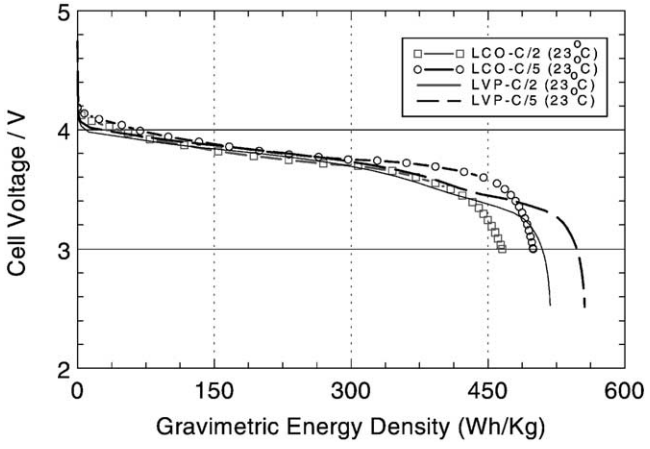

Fig. 10. Discharge curves for LVP||graphite and LCO||graphite cells at *C*/5 and *C*/2 rates (23 °C).

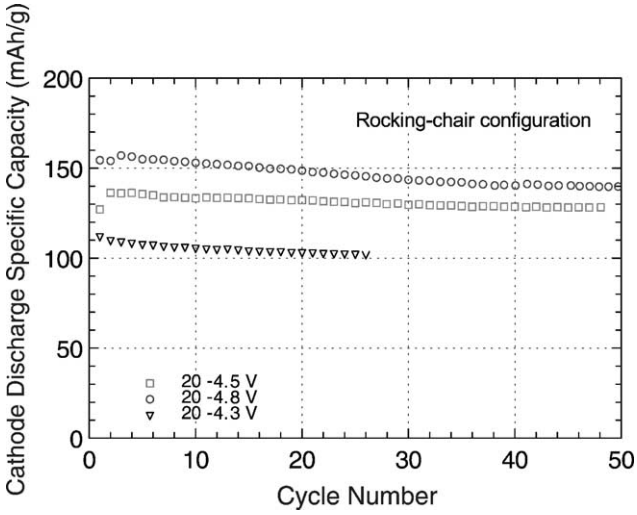

Fig. 12. Specific discharge capacities vs. cycle number for LVP||graphite cells: (○) 3.0–4.8 V, (□) 3.0–4.5 V, (▽) 3.0–4.3 V.

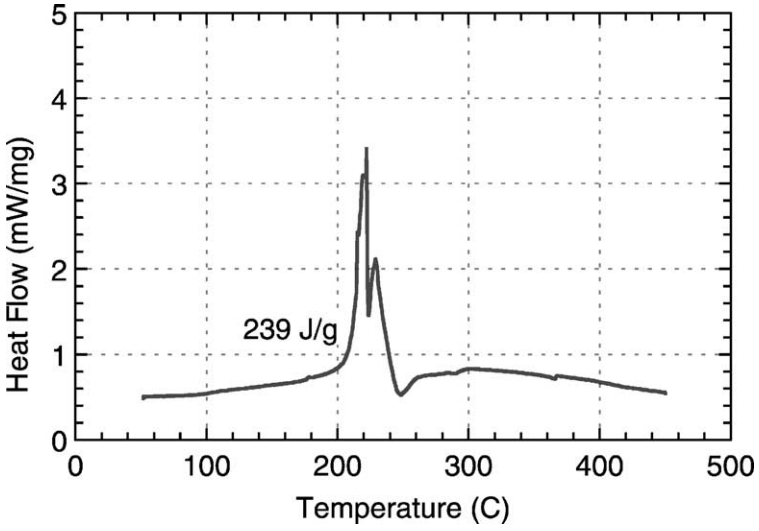

Fig. 13. DSC curve of fully charged LVP cathode to 4.8 V in the presence of electrolyte (heating rate, 5 °C/min).

4. Conclusion

Monoclinic $Li_3V_2(PO_4)_3$ can be synthesized from V_2O_5 using either hydrogen or carbon as the reducing agent. Structural analysis has shown that it is iso-structural with the monoclinic Fe equivalent. When the amount of lithium removed from the structure is limited to 2 mol/FU, a good reversibility is observed. The redox couple V^{3+}/V^{4+} is, therefore, attractive for lithium rechargeable batteries providing a system with an average voltage of 3.8 V versus Li/Li^+ and a reversible capacity of 130 mAh/g. Extraction of the last lithium, V^{4+}/V^{5+}, which takes place at 4.6 V versus Li/Li^+ appears to be energetically unfavorable and, hence exhibits a larger overvoltage. However, on the subsequent discharge, all of the extracted lithium ($Li_2V_2(PO_4)_3 \rightarrow Li_{\approx 0.3}V_2(PO_4)_3$ is fully re-inserted back in a single step. Also, at the end of charge, when approximately three lithiums have been extracted, XRD showed the presence of a monoclinic phase. Upon discharge, however, the original structure is recovered. The lithium-ion batteries showed very good charge–discharge reversibility and a capacity retention of 150 mAh/g for the fully de-lithiated samples (lithium-ion cells). Furthermore, the rate dependence performance exceeded that of $LiCoO_2$ under the same conditions, in particular at −10 °C. Combined with an excellent thermal stability and ease of synthesis, lithium vanadium phosphate can be a very viable candidate for higher energy density and power demanding lithium-ion batteries.

References

[1] S. Megahed, B. Scrosati, J. Power Sources 51 (1994) 79.
[2] M. Armand, Materials for Advanced Batteries, in: D.W. Murphy, J. Broadhead, B.C.H. Steele (Eds.), Plenum Press, New York, 1980, p. 145.
[3] R. Koksbang, J. Barker, H. Shi, M.Y. Saidi, Solid State Ion. 84 (1996) 1.
[4] S. Okada, K.S. Nanjundaswamy, A. Manthiram, J.B. Goodenough, H. Arai, J. Yamaki, in: Proceedings of the 36th Power Sources Conference, vol. 110, Cherry Hill, NJ, June 1994.
[5] A.B. Bykov, A.P. Chirkin, L.N. Demyanets, S.N. Doronin, Solid State Ion. 38 (1990) 31.
[6] P.A. Kokkoros, Miner. Petro. Mitt. 10 (1965) 45.
[7] K. Nassau, H.J. Levinstein, J. Phys. Chem. Mat. 26 (1965) 1805.
[8] A.W. Sleight, L.H. Brixner, J. Solid State Chem. 7 (1973) 172.
[9] J. Gopalakrishnan, K. Kasthuri Rangan, Chem. Mater. 4 (1992) 745.
[10] S. Okada, H. Arai, K. Asakura, Y. Sakurai, J. Yamaki, K.S. Nanjundaswamy, A.K. Padhi, C. Masquelier, J.B. Goodenough, Prog. Batter. Battery Mater. V16 (1997) 302.
[11] J. Barker, M.Y. Saidi, US Patent 5,871,866 (1999).
[12] A.H. Thompson, J. Electrochem. Soc. 126 (1979) 608.
[13] J. Barker, Synth. Met. 32 (1989) 43.
[14] T. Jacobsen, K. West, S. Atlung, J. Electrochem. Soc. 126 (1979) 608.
[15] O. Tillement, M. Quarton, J. Electrochem. Soc. 140 (1993) 1870.
[16] D. Morgan, G. Ceder, M.Y. Saidi, J. Barker, H. Huang, J. Swoyer, G. Adamson, Chem. Mat. 14 (2002) 4684.
[17] K.S. Nanjundaswamy, A.K. Padhi, J.B. Goodenough, S. Okada, H. Ohtsuka, H. Arai, J. Yamaki, Solid State Ion. 92 (1996) 1.
[18] J. Barker, M.Y. Saidi, J. Swoyer, J. Electrochem. Soc., Solid State Lett. 6 (3) (2003) A53.